Automated road markings extraction from mobile laser scanning data

Pankaj Kumar*, Conor P. McElhinney, Paul Lewis, Timothy McCarthy

National Centre for Geocomputation (NCG), National University of Ireland Maynooth (NUIM), Maynooth, Co. Kildare, Ireland

ABSTRACT

Road markings are used to provide guidance and instruction to road users for safe and comfortable driving. Enabling rapid, cost-effective and comprehensive approaches to the maintenance of route networks can be greatly improved with detailed information about location, dimension and condition of road markings. Mobile Laser Scanning (MLS) systems provide new opportunities in terms of collecting and processing this information. Laser scanning systems enable multiple attributes of the illuminated target to be recorded including intensity data. The recorded intensity data can be used to distinguish the road markings from other road surface elements due to their higher retro-reflective property. In this paper, we present an automated algorithm for extracting road markings from MLS data. We describe a robust and automated way of applying a range dependent thresholding function to the intensity values to extract road markings. We make novel use of binary morphological operations and generic knowledge of the dimensions of road markings to complete their shapes and remove other road surface elements introduced through the use of thresholding. We present a detailed analysis of the most applicable values required for the input parameters involved in our algorithm. We tested our algorithm on different road sections consisting of multiple distinct types of road markings. The successful extraction of these road markings demonstrates the effectiveness of our algorithm.

© 2014 Elsevier B.V. All rights reserved.

1. Introduction

Road user safety may be affected by existence and condition of safety interventions along the route corridor. A well designed and maintained route corridor assists in driver safety as well as in the efficient use of overall network in terms of route navigation (ETSC, 1997). Road markings play an important role in reducing accident frequency and severity as they provide guidance and instruction to the road users for safe and comfortable driving. They are intended to direct traffic by indicating the direction of travel, warn road users about specific obstacles or hazards and define the territorial limit for traffic flows (Gatti et al., 2007). Road markings are retro-reflective surfaces having an ability to reflect most of the incident light back to its originating source. These markings retain their visibility criteria in day and night. Road markings may deteriorate due to intensive use or suffer from reduced visibility due to many factors such as occlusions that arise from vegetation growth. Road markings are required to be located, measured, classified and recorded in a timely, cost effective manner in order to schedule maintenance and ensure maximum safety conditions for road users (Kumar, 2012).

Various safety schemes and standards such as the Road Safety Audit (RSA), Road Safety Inspection (RSI) and Network Safety Management (NSM) are implemented to qualitatively estimate potential road safety issues along the route corridor. The aim of these road safety assessment methodologies is to identify the elements of the road that may present a safety concern and explore the various opportunities to eliminate identified safety concerns (ETSC, 1997). The information collected through these surveys is sometimes incomplete and insufficient for qualitative estimation of potential road safety issues. It can also be time consuming and expensive to conduct these inspections on a large scale. A recent research call highlighted the requirement for common evaluation tools and implementation strategies in carrying out these inspections and assessing risk along route corridors (Pecharda et al., 2009). One research project European Road Safety Inspection (EuRSI) demonstrated that terrestrial Mobile Mapping Systems (MMS) could be used to collect physical route corridor information for rapid safety analysis (McCarthy and McElhinney, 2010).

Mobile mapping refers to a methodology of collecting geospatial data using mapping and navigation sensors that are mounted rigidly onboard a mobile platform (Schwarz and El-sheimy, 2007; Barber et al., 2008). Multi sensor integrated mapping technology has enabled rapid and cost effective acquisition of georeferenced information about road network environments (Li and Chapman,

* Corresponding author. Tel.: +353 17086180.

2008). Their initial development was primarily driven by advances in digital cameras and navigation technologies. Later, laser scanning systems were integrated with MMSs which facilitated more accurate and dense collection of 3D point cloud data. The applicability of mobile laser scanning (MLS) systems continues to prove their worth in route corridor mapping due to their rapid, continuous and cost effective 3D data acquisition capability. MLS systems usually record the intensity data which can be used to distinguish road markings that produce high reflectivity due to their retro-reflective property. Knowledge of the location, dimension and condition of road markings can be useful for road safety, route network maintenance and driver assistance systems. In Kumar et al. (2013), we presented an automated algorithm for extracting road edges from MLS data. The automated road edge extraction algorithm is applied to estimate road boundaries from LiDAR data. The output road boundaries are then used to identify the LiDAR points that belong to the road surface. Knowledge of the road surface area facilitates a more efficient and accurate extraction of road markings. In this paper, we will present an automated algorithm for extracting road markings from MLS data. The algorithm is based on applying a range dependent thresholding function to the intensity values to extract road markings from MLS data. In Section 2, we review various approaches developed for extracting road markings from LiDAR data. In Section 3, we present a stepwise description of our automated road marking extraction algorithm. In Section 4, we present our analysis to find the most applicable values of input parameters required to automate the road marking extraction algorithm. In Section 5, we test our algorithm on various road sections, demonstrating the successful extraction of different types of road markings. We discuss the results following validation of the road marking extraction process in Section 6. Finally, we conclude the paper in Section 7.

2. Literature review

MLS systems enable the acquisition of an accurately georeferenced set of dense LiDAR point cloud data. Because of the fundamental structure and intrinsic properties of LiDAR data, it enables more efficient and accurate road feature extraction approaches to be explored. Apart from facilitating the collection of 3D positional information, laser scanning systems record a number of attributes including intensity, pulse width, range and multiple echo which can be used for reliable and precise extraction of different spatial objects. The pulse width from the laser scanning system refers to a recorded time difference between half maximum amplitudes of the pulse (Kumar, 2012). The pulse width attribute can be used to classify terrain objects as its values vary with the surface roughness (Lin and Mills, 2010). The methods developed for segmenting LiDAR data are mostly based on the identification of planar or smooth surfaces and the classification of point cloud data based on its attributes (Vosselman, 2009). In a related area, several methods have been developed over the past decade for extracting urban building features from LiDAR data (Hammoudi et al., 2009; Rutzinger et al., 2009; Kabolizade et al., 2010; Haala and Kada, 2010). Other approaches have been based on extracting road and its environment from LiDAR data. Clode et al. (2004) and Hu et al. (2004) segmented Airborne Laser Scanning (ALS) data into road and non-road based on elevation and intensity attributes, while Samadzadegan et al. (2009) used first echo, last echo, range and intensity attributes to classify the ALS points into road objects. Mumtaz and Mooney (2009) used ALS elevation and intensity attributes to extract spatial information about buildings, trees, roads, poles and wires in the route corridor environment. Lam et al. (2010) extracted roads through fitting a plane to 3D terrestrial mobile point cloud data and then used the extracted information to distinguish lamp posts, power line posts and power lines by

employing context based constraints. Pu et al. (2011) segmented MLS data into traffic signs, poles, barriers, trees and building walls based on spatial characteristics of point cloud segments like size, shape, orientation and topological relationships. Similarly, Zhou and Vosselman (2012) used elevation attribute, while McElhinney et al. (2010) and Kumar et al. (2013) employed elevation, intensity and pulse width attributes to extract road edges in multiple route corridor environment from MLS data.

LiDAR data provides an intensity attribute which depends upon the range, incidence angle of the laser beam and surface characteristics. The intensity values are required to be normalised with respect to these factors prior to the threshold implementation or the use of a range dependent threshold approach is recommended for segmentation or feature extraction (Vosselman, 2009). Most of the approaches used for normalising their values are based on using models and data driven methods (Pfeifer et al., 2008; Jutzi and Gross, 2009; Oh, 2010) while other approaches are based on using external reference targets of known reflectivity behaviour (Kaasalainen et al., 2009; Vain et al., 2009). The intensity attribute can be used to distinguish road markings from the road surface. Precise extraction of road markings from LiDAR data has drawn limited attention from the research community. Jaakkola et al. (2008) estimated road markings by first performing a radiometric correction of the LiDAR intensity data using a second order curve fitting function. Finally, road markings were estimated by applying a threshold and morphological filtering methods. Toth et al. (2007, 2008) used road markings as ground control for assessing the positioning quality of ALS data. The search window for finding the road markings in the LiDAR data was reduced by making use of the Global Positioning System (GPS) survey data collected over the pavement. The road markings were extracted by thresholding the LiDAR intensity values. Later, extracted road markings were compared with the GPS survey data to assess the quality of the LiDAR points. Vosselman (2009) described the use of a range dependent thresholding for extracting road markings from MLS data. The thresholded road marking points were grouped using connected component analysis and then full outlinings of the road markings were obtained by fitting predefined shapes to the grouped segments. Chen et al. (2009) developed a method for extracting lane markings from the MLS data. The road surface was detected by discarding the non-road points based on the standard deviation values of LiDAR elevation attribute and then candidate lane marking points were localised by applying a threshold to the intensity values of road surface points. The lane markings were clustered by applying the Hough transform to 2D binary image generated from candidate points and were further refined using trajectory and geometry check constraints. Smadja et al. (2010) developed an algorithm for extracting roads from MLS data based on the detection of slope break points coupled with the RANdom SAmple Consensus (RANSAC) algorithm. The estimated road information was used to extract road markings by applying a threshold approach to the LiDAR intensity data. Butler (2011) developed an automated approach to extract road markings from MLS system. The road marking points were extracted by thresholding the LiDAR intensity attribute and then output points were filtered based on their neighbourhood within a specified threshold distance. The road marking points were clustered and convex hulls were fitted to them. Yang et al. (2012) described an automated approach for extracting road markings from MLS data. In their approach, 2D image was generated from LiDAR point cloud data and then road markings were filtered by applying threshold to the LiDAR intensity and elevation values. Finally, the outlines of road markings were extracted based on priori knowledge of the shapes and arrangement of the road markings.

The majority of methods developed for extracting road markings are based on applying a threshold to the LiDAR intensity values. The development of a robust threshold approach will provide a
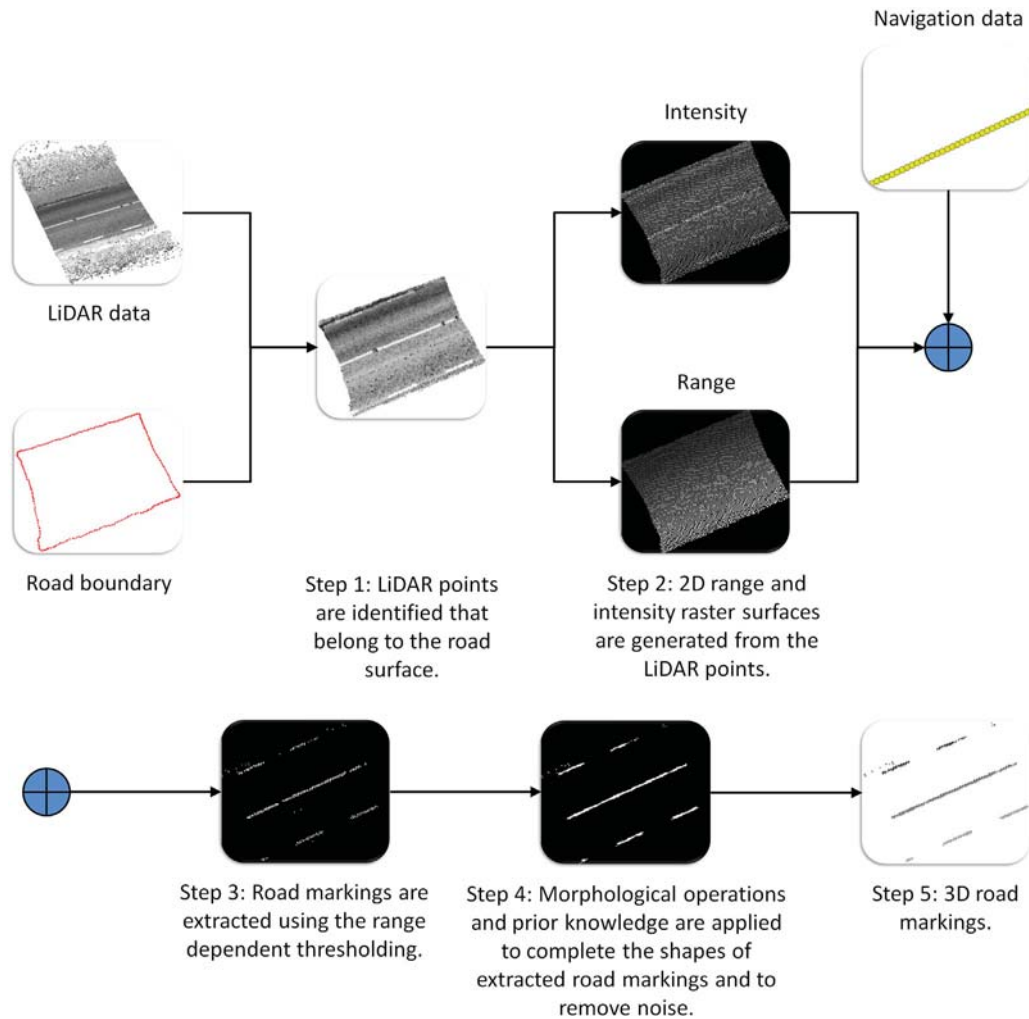
Fig. 1. Road marking extraction algorithm.

more precise extraction of road markings. The factors that affect the values of intensity attribute are required to be addressed prior to their use for road markings extraction. A threshold applied to the intensity values often introduces some of the other road surface elements, which needs to be removed. A priori knowledge of the road boundaries and its surface will facilitate a more efficient extraction of road markings. In the next section, we present our automated road marking extraction algorithm.

3. Algorithm

In Kumar et al. (2013), we presented an automated algorithm for extracting road edges from MLS data. We input n number of $30\,m \times 10\,m \times 5\,m$ LiDAR and n number of $10\,m$ navigation data sections in the road edge extraction algorithm. The dimensions of input data sections were selected based on empirical tests as they impact the process efficiency in terms of computational cost (Kumar, 2012; Kumar et al., 2013). The algorithm outputs road boundary which is used to identify the LiDAR points that belong to the road surface. We apply our automated road making extraction algorithm to the estimated road surface LiDAR points which facilitates a more efficient and accurate extraction of road markings. Our automated road marking extraction algorithm is based on the assumption that the intensity values of the laser returns from the road markings are higher than those from other road surface elements. We expect to extract

these road markings by applying a range dependent thresholding to the intensity values. We convert the LiDAR intensity and range attributes into 2D raster surfaces which allow us to apply morphological operations to them. A workflow of the road marking extraction algorithm is shown in Fig. 1. In the following sections, we describe the various processing steps involved in our algorithm.

3.1. Road surface estimation

We input the LiDAR data and the road boundary estimated using our automated road edge extraction algorithm. In Step 1 of our road marking extraction algorithm, we use the road boundary to identify the LiDAR points that belong to the road surface. A road boundary is laid over the LiDAR data such that the points outside the road boundary are removed, while the inner points are retained to estimate the road surface.

3.2. 2D raster surface generation

We use LiDAR intensity and range attributes in our algorithm to extract the road markings. In Step 2 of our algorithm, we generate 2D intensity and range raster surfaces from the LiDAR data using a cell size, c parameter. An optimal value of c parameter is selected based on a detailed analysis provided in Section 4.1. The value of each cell in the raster surface is estimated as the average of the intensity and range values of the LiDAR points that fall within
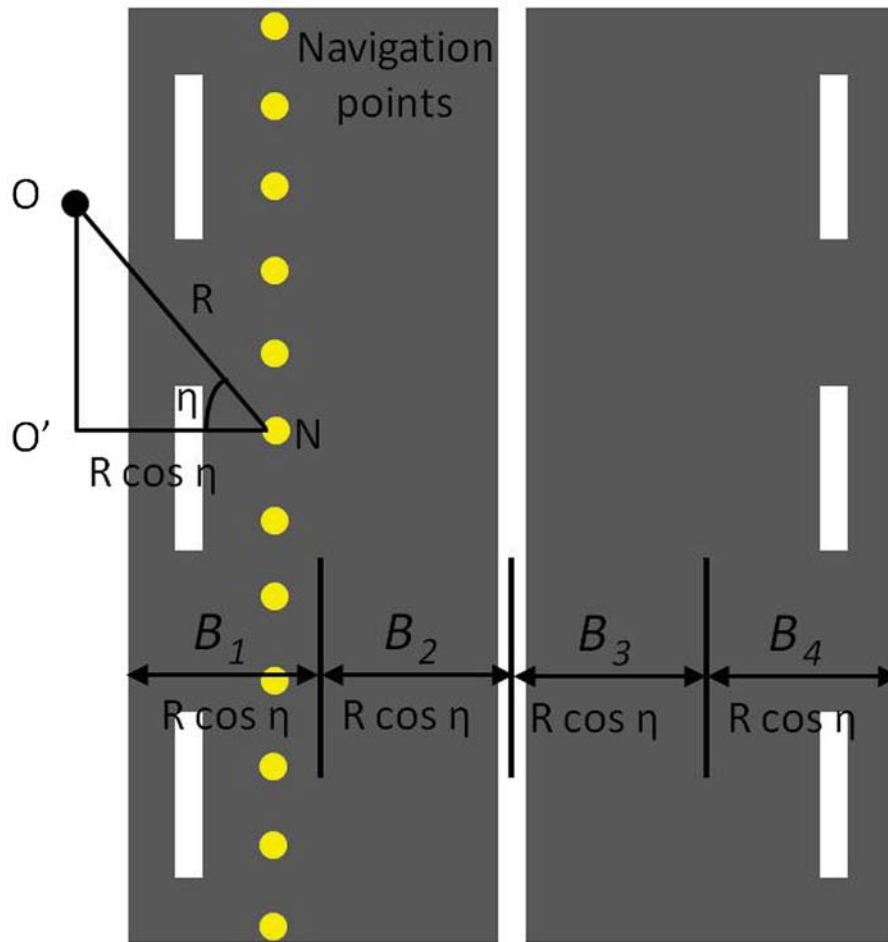
Fig. 2. Navigation data is used to select a range value to apply multiple threshold values to the intensity raster surface.

the 2D boundary of the cell. The intensity and range raster surface values are normalised with respect to their global minimum and maximum, and converted into an 8-bit data type. This will allow for the use of one set of values for all road sections.

3.3. Range dependent thresholding

Road markings are generally more reflective than the road surface. This results in the intensity values of the laser returns from the road markings being higher than the background surface. However, apart from the reflectivity of the illuminated surface, there are two other factors affecting the intensity values, the range and the incidence angle of the laser beam. These factors need to be addressed in any algorithm extracting road markings. In Step 4 of our algorithm, we apply range dependent thresholding to the intensity raster surface. We use the navigation data to select a range value that is used to apply multiple threshold values. In most MLS systems, the laser scanner is mounted on a mobile van at some horizontal and vertical inclined position in order to produce rich 3D information. Let us suppose that a laser scanner is mounted on the back of the mobile van at a η inclination angle from both the horizontal and vertical axes of the vehicle. This inclined position modifies the initial scanning point from directly below the scanner to the position, O, shown in Fig. 2. R is the range of a laser beam from the navigation point N to the initial scanning point O. The transverse range from the point N to O' is estimated as $R\cos\eta$. For each laser return, we replace their range value with the new transverse range value using the inclination angle η. We use the estimated transverse range value

$R\cos\eta$ to divide the intensity raster surface into different blocks which allows us to threshold the intensity values based on their range from the scanner.

We apply a different threshold value to each block of the intensity raster surface to deal with the range and incidence angle factors that affect intensity values. The road surface is usually constructed with a non-planar shape, shown in Fig. 3. This surface is engineered to allow rain water to run off the road surface to reduce water pooling which can damage the road surface over time. This type of road surface might influence the incidence angle of the laser beam, resulting in a change in intensity returns as the range increases. We apply the threshold values T_{I1}, T_{I2}, T_{I3} and T_{I4} to data in the blocks B_1, B_2, B_3 and B_4, respectively, to extract road markings. We select a single optimal value of threshold, T_I empirically and use it to estimate the values of T_{I1}, T_{I2}, T_{I3} and T_{I4}. A detailed analysis on the selection of the range dependent threshold values is provided in Section 4.2.

3.4. Morphological operations

The extracted road markings from Step 3 may be incomplete and contain other road surface elements that are introduced through the use of thresholding. To overcome this, we make a novel use of binary morphological operations (Haralick and Shapiro, 1992) and priori knowledge of the dimensions of road markings in Step 4 of our algorithm. Their implementation involves three processes. In the first process, the thresholded raster surface is converted into a binary image and then we apply the dilation operation to the
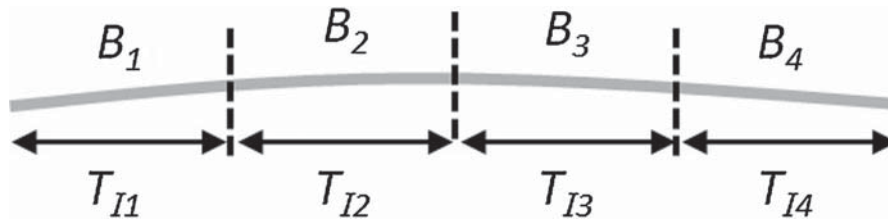
Fig. 3. Side view of the non-planar road surface.

binary image in which a structuring element is placed over the cells of the image. The purpose of dilation is to use the structuring element to grow cells with a value of 1 in order to fill in any holes. A structuring element consists of a binary matrix that represents the selected shape and size. Examples of structuring elements with different shapes and sizes are shown in Fig. 4. A central element of the matrix represents an origin and the elements with a value of 1 describe a neighbourhood of the structuring element. The origin of the structuring element is positioned over each cell in the binary raster surface to dilate that cell along the neighbourhood of the structuring element.

A linear shaped structuring element is used to dilate the cells of each road marking. We choose a linear shape for the structuring elements due to the general linear patterns of road markings. The linear shaped structuring element is used with a ϕ' angle that is calculated from the average heading of the mobile van along the road section under investigation. This angle is used in order to dilate the road markings along the longitudinal direction. A process of calculating the ϕ' angle from the average heading angle of the mobile van, θ, is described in Fig. 5. The θ angle provides the direction of the mobile van's trajectory with respect to the north direction and the ϕ' angle is measured in the anticlockwise direction from the horizontal axis. If the value of θ angle lies in between 0° and 90°, then the ϕ' angle is estimated as $90° - \theta$ in the anticlockwise direction as shown in Fig. 5(a). Similarly, the ϕ' angle can be estimated for other possible values of the θ angle as shown in Fig. 5(b)–(d).

The l, length of the linear shaped structuring element is selected empirically. We use the same value in each road section, which allows us to automate the morphological operation in our algorithm. An example of the input binary image is shown in Fig. 6(a). The input binary image is dilated using a linear shaped structuring element with $l = 9$ and $\phi' = 38.37°$ as shown in Fig. 6(b). The use of dilation operation fills the holes and completes the shapes of road markings in the input binary image.

In the second process, we group cells into objects in the dilated image using connectivity. If a cell has a value of 1 then it is connected to the cells whose values are 1 and are directly above, below, left or right of that cell. We calculate the length and average width values of each object in the dilated image. Objects whose length and average width values are less than length threshold, T_L and width threshold, T_W are considered as other road surface elements and are removed from the image. An example of road surface cells removed from the dilated image is shown in Fig. 6(c).

In the third process, we apply an erosion operation to the dilated image in order to retain the original boundary shape of the road markings. In an erosion operation, cells are removed from the road marking cells using a structuring element. The linear shaped structuring element used for dilation is also applied to erode the road markings. An example of the dilated road markings eroded using the linear shaped structuring element with $l = 9$ and $\phi' = 38.37°$ angle is shown in Fig. 6(d). In this way, the combined use of morphological operations and priori knowledge of the dimensions of road markings is able to complete their shapes and to remove other road surface elements.

3.5. 3D road markings

In Step 5 of our algorithm, we extract the 3D road markings using the 2D output. The original 3D LiDAR points which are contained within the 2D road marking cell boundaries are extracted. In the next section, we present our analysis of the input parameters used to automate our road marking extraction algorithm.
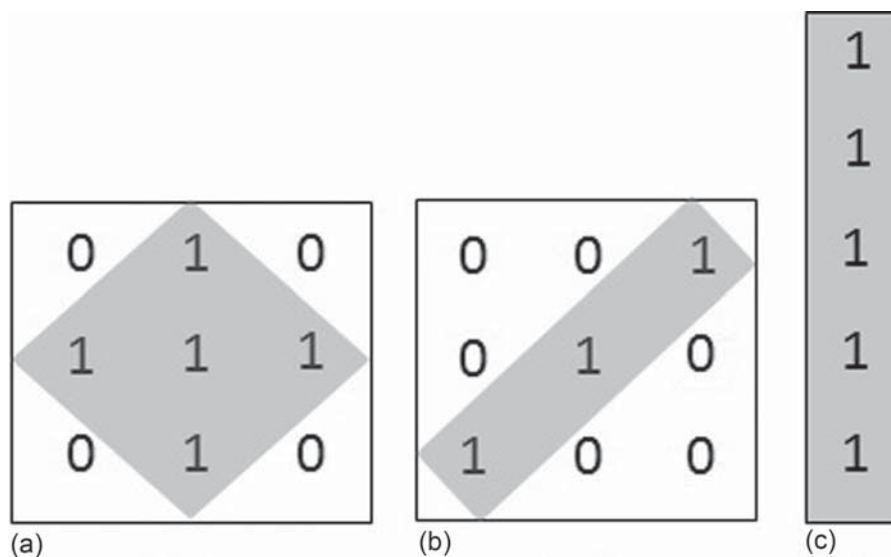

Fig. 4. Structuring elements: (a) diamond shaped with radius, $r = 1$, (b) linear shaped with length, $l = 3$ and angle, $\phi' = 45°$ and (c) linear shaped with length, $l = 5$ and angle, $\phi' = 90°$.
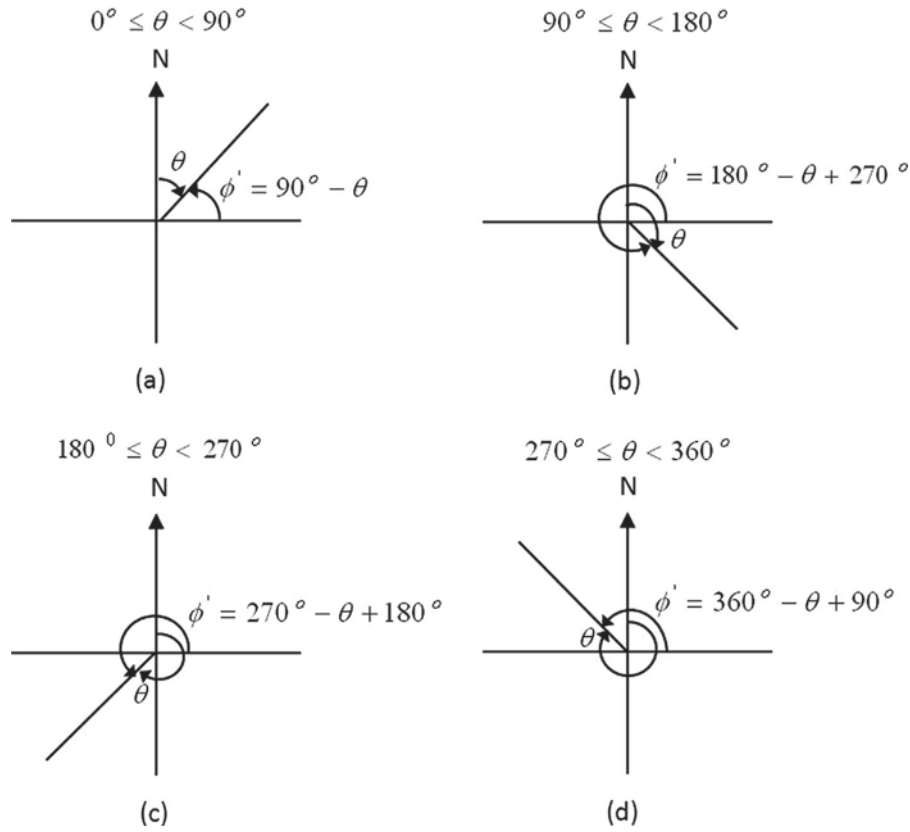
Fig. 5. Estimation of ϕ' angle of the linear shaped structuring element from the average heading angle of the mobile van, θ, along the road section that can lie in between (a) 0° and 90°, (b) 90° and 180°, (c) 180° and 270° and (d) 270° and 360°.

4. Parameter analysis

Our road marking extraction algorithm requires two input parameters, the cell size value for converting the LiDAR data into 2D raster surfaces and the range dependent threshold value. To implement an automated algorithm, we need the most applicable value for each of these. In the following sections, we will detail our recommended values and show the effect of changing these.

4.1. Optimal cell size parameter

We convert the LiDAR data into 2D raster surfaces as described in Section 3.2. Each cell in the raster surface has a physical dimension.
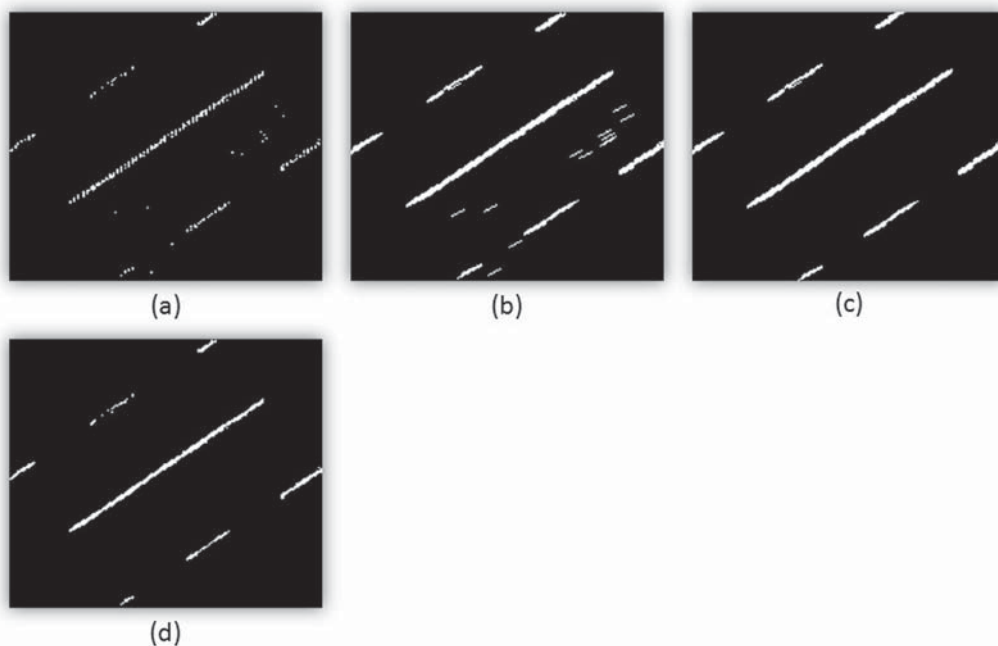

Fig. 6. Morphological operation: (a) input binary image, (b) dilated image, (c) road surface cells removed and (d) eroded image.
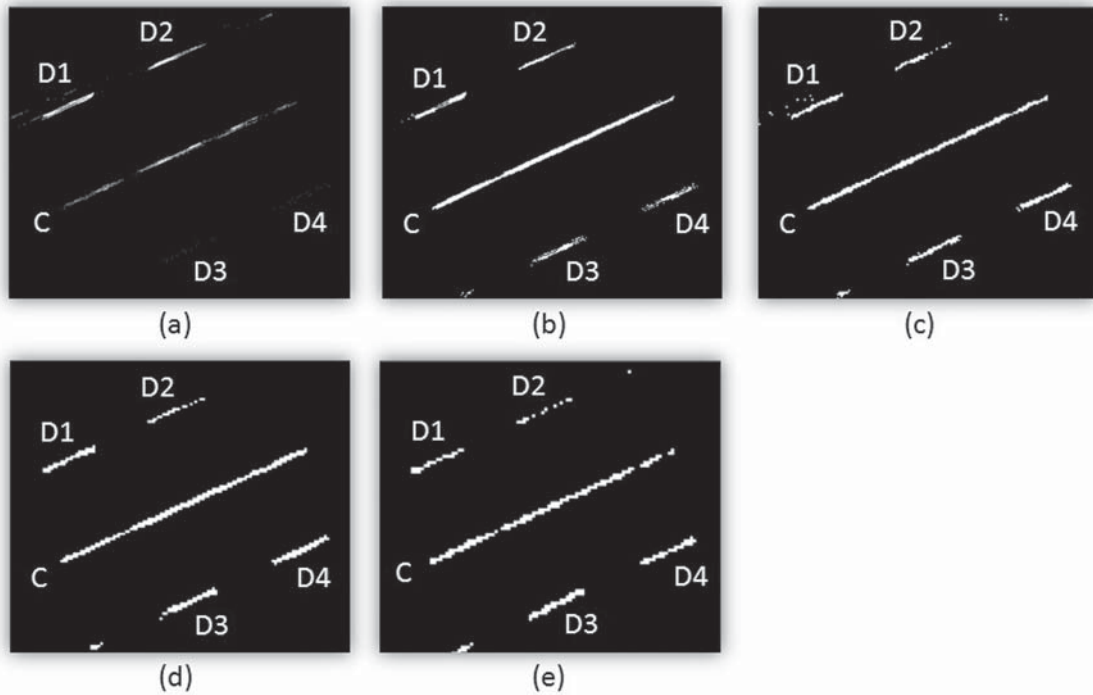
Fig. 7. Road markings extracted with (a) 0.01 m², (b) 0.04 m², (c) 0.06 m², (d) 0.08 m² and (e) 0.1 m² cell size in the five test cases of the optimal cell size analysis.

The cell size influences the average intensity and range values of the cell which in turn affects the output result in terms of accuracy and computational cost. Our road marking extraction algorithm is primarily based on range dependent thresholding which is not computationally expensive. Therefore, we considered accuracy as the main criteria for cell size selection. To find its optimal value, we analysed the performance of our road marking extraction algorithm in raster surfaces generated with different cell sizes. We selected one 10 m section of rural road which contained broken and continuous line markings over its surface. To process this road section, we used $n = 1$ number of 30 m $\times$ 10 m $\times$ 5 m section of LiDAR data and $n = 1$ number of 10 m section of navigation data. The data were collected using the eXperimental Platform (XP-1) MMS which has been designed and developed at National University of Ireland Maynooth (Kumar et al., 2010, 2011).

The automated road edge extraction algorithm was applied to the selected road section to obtain output road boundary. We then applied our automated road marking extraction algorithm by considering five test cases in which raster surfaces were generated from the LiDAR intensity and range attributes with different cell sizes. The parameters used in the algorithm in the five test cases are shown in Table 1. The cell sizes were selected with decreasing and increasing values based on an average point spacing of 0.08 m² in the LiDAR points while the value of l parameter was chosen in accordance with the respective cell size selected in each case. The ϕ' angle was calculated as $90° - \theta$ while the values of T_L and T_W were selected based on minimum possible 0.5 m length and 0.1 m

Table 1
The parameters used in the five test cases of the optimal cell size parameter analysis.

Test case	c (m²)	T_I	l	ϕ' (°)	T_L (m)	T_W (m)
1	0.01	70	51	24.23	1	0.1
2	0.04	70	13	24.23	1	0.1
3	0.06	70	9	24.23	1.02	0.1
4	0.08	70	7	24.23	1.04	0.1
5	0.1	70	5	24.23	0.9	0.1

width of the road markings used in the real world road environment (Transport, 2010). The value of T_I was modified as a function of range and applied to four blocks of the intensity raster surface. We used a similar value of T_W in each test case as the cells were not dilated along the transverse direction. The road markings extracted in the five test cases are shown in Fig. 7.

In order to carry out a comparative analysis, we calculated the length and average width of the final extracted road markings in the five cases. We considered four broken line markings named as $D1$, $D2$, $D3$ and $D4$ and one continuous line marking named as C, shown in Fig. 7. The calculated length, L and average width, W values are listed in Table 2. We found a standard length and width of the five road markings from the traffic signs manual (Transport, 2010). We compared the extracted L and W values of the road markings with the expected standard dimensions. For cell sizes 0.08 m² and 0.1 m², the W values of the road markings were generally found to be more than their standard values. For the 0.06 m² cell size, the L

Table 2
Length and average width values of the extracted road markings in the five test cases of the optimal cell size analysis.

| Road markings (standard $L \times W$)	0.01 m²		0.04 m²		0.06 m²		0.08 m²		0.1 m²	
	L	W	L	W	L	W	L	W	L	W
$D1$ (2 m $\times$ 0.15 m)	1.75 m	0.12 m	1.68 m	0.12 m	1.68 m	0.12 m	1.68 m	0.16 m	1.70 m	0.13 m
$D2$ (2 m $\times$ 0.15 m)	1.84 m	0.07 m	1.84 m	0.07 m	1.80 m	0.08 m	1.84 m	0.08 m	1.80 m	0.07 m
$D3$ (2 m $\times$ 0.15 m)	1.71 m	0.002 m	1.80 m	0.10 m	1.80 m	0.13 m	1.84 m	0.17 m	1.80 m	0.20 m
$D4$ (2 m $\times$ 0.15 m)	1.78 m	0.002 m	1.80 m	0.08 m	1.80 m	0.14 m	1.84 m	0.18 m	1.80 m	0.16 m
C (8.6 m $\times$ 0.15 m)	7.80 m	0.034 m	7.84 m	0.145 m	7.86 m	0.141 m	7.92 m	0.17 m	7.90 m	0.16 m
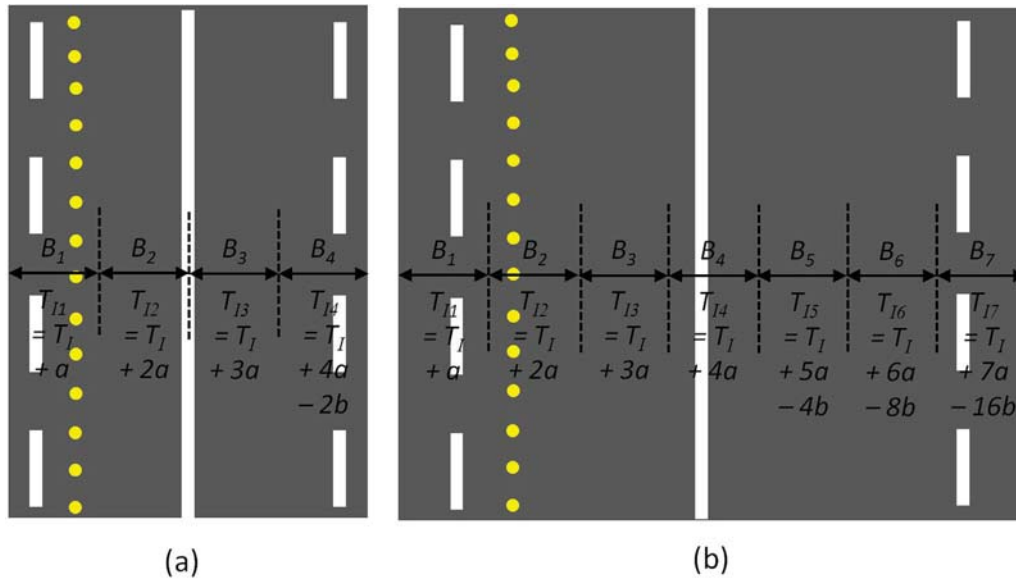
Fig. 8. Range dependent thresholding applied to the intensity raster surface in the road section with (a) narrower and (b) greater width.

and W values of the road markings were closest to their standard values. Thus, we selected $0.06\,m^2$ cell size as the most applicable value to generate 2D intensity and range raster surfaces from the LiDAR data.

4.2. Range dependent threshold parameter

After selecting the optimal cell size, the final parameter requiring selection is the range dependent threshold. The aim of this analysis was to determine a method for automatically selecting this threshold value irrespective of the road dimension. We use the navigation data to select the range value that is used to divide the intensity raster surface into different blocks. In a road section with a narrower width, the intensity raster surface was divided into four blocks, shown in Fig. 8(a). In a road section with a greater width, the intensity raster surface was divided into seven blocks, shown in Fig. 8(b). We selected a single threshold value $T_I = 70$ empirically and modified it as a function of the range. We applied a $T_I + ma$ threshold to each block of the intensity raster surface, where $a = 10$ and m represents a block number. We applied the $T_I + ma - nb$ threshold to the blocks after the centre of the road, where $b = 5$ and $n = 1, 2, 4, 8, \ldots$ representing an integer for the third, fourth, fifth, sixth, etc. blocks, respectively. The threshold values applied before the centre of the road were consecutively increased with the ma term, as the road surface in those blocks begins to orient towards the laser scanner. The threshold values applied after the centre of

Table 3
The parameters used in the road marking extraction algorithm.

Parameter	Value
c	$0.06\,m^2$
T_I	70
l	9
T_L	$1.02\,m$
T_W	$0.1\,m$

the road were increased with the term ma and then decreased with the nb term to account for the increased range and the change in surface orientation. The purpose of finding these variables was to automate the process of applying the range dependent thresholding to the intensity raster surface.

To demonstrate the importance of the empirically selected value of T_I, we applied its lower, optimal and higher value to the intensity raster surface as 55, 70 and 90. Each value was modified as a function of the range in accordance with the aforementioned formulae and used to extract the road markings, shown in Fig. 9(a)–(c). The use of a lower threshold value led to the extraction of road markings with large areas of other road surface elements, while its higher value removed those elements at the expense of extracting all the road markings. Thus, the selection of an optimal threshold value is essential for the robust extraction of road markings. In the next section, we test our automated road marking extraction algorithm on various road sections.
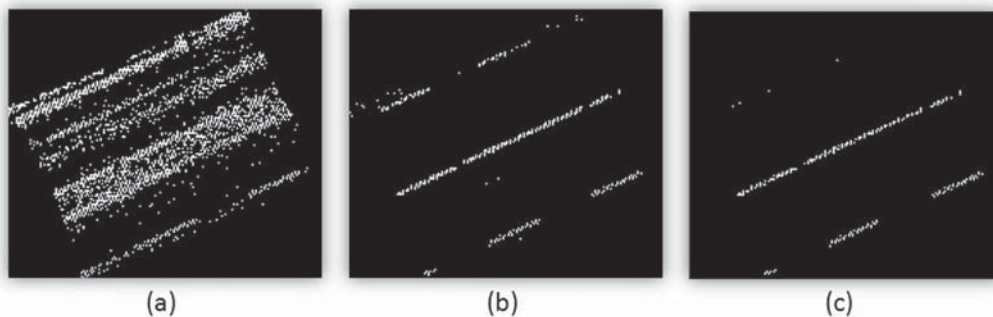

Fig. 9. Road markings extracted using the (a) lower, (b) optimal and (c) higher value of T_I applied to the intensity raster surface.

Fig. 10. Digital image of (a) first, (b) second, (c) third, (d) fourth, (e) fifth and (f) sixth road section (geographic locations: (a) 53°34′28.07″ N 7°10′13.76″ W, (b) 53°36′33.43″ N 7°5′46.96″ W, (c) 53°34′50.546″ N 7°8′57.62″ W, (d) 53°39′19.225″ N 7°31′9.792″ W, (e) 53°33′49.878″ N 7°21′24.148″ W and (f) 53°35′30.558″ N 7°22′28.428″ W).

5. Experimentation

We selected six sections of road to test our road marking extraction algorithm. These six sections covered 140 m of rural, urban and national primary roads, which contained six distinct types of road markings to demonstrate the effectiveness of our algorithm. The processed data were collected with the XP-1 MMS along these road sections. The first 50 m section of rural road and second 50 m section of urban road consisted of broken and continuous line markings, shown in Fig. 10(a) and (b). The third 10 m section of rural road consisted of word, broken and continuous line markings, fourth 10 m section of urban road consisted of zig-zag markings, fifth 10 m section of national primary road consisted of hatch and broken line markings while sixth 10 m section of national primary road consisted of arrow and broken line markings as can be seen in Fig. 10(c)–(f), respectively. To process each 50 m road section, we used $n = 6$ number of 30 m × 10 m × 5 m sections of LiDAR data and $n = 6$ number of 10 m section of navigation data and to process each 10 m road section, we used $n = 1$ number of 30 m × 10 m × 5 m sections of LiDAR data and $n = 1$ number of 10 m section of navigation data.

We applied our automated road marking extraction algorithm to each road section using parameters as shown in Table 3. The ϕ' angle was calculated as $90° - \theta$ in each navigation section of the first and second road sections while $180° - \theta + 270°$ in each navigation section of the third, fourth, fifth and sixth road sections. The value of θ angle in each navigation section of the road sections are shown in Table 4. The original LiDAR data and extracted road markings of the

Table 5
Validation of extracted road marking test results.

| Road markings	Manual inspection		Extracted result	
	Objects	Points	Objects	Points
Continuous line	3	5280	3	5007
Broken line	71	8953	64	7718
Words	8	948	8	786
Zig-zag	3	1816	2	1299
Hatch	1	1077	1	1065
Arrow	2	1076	2	1060
Total	88	19150	80	16935

six road sections are shown in Figs. 11–13. In the next section, we validate the road marking experimental results and discuss them.

6. Results & discussion

We validated the extracted road marking results through a quantitative and qualitative assessment based on manual inspection. Our error assessment was focused on the number and shape detection of the extracted road marking objects. We manually counted a number of road marking objects and a number of 3D LiDAR points in each object as shown in Table 5. We found 88 number of road marking objects and 19150 number of road marking points in the tested road sections. Our road marking extraction algorithm was able to correctly extract a total of 80 road markings but failed to detect 8 road markings. Similarly, the algorithm extracted 16935 number of road marking points while 7458 points

Table 4
Average heading angle, θ, in each navigation section of the six road sections.

| Navigation section	First road section	Second road section	Third road section	Fourth road section	Fifth road section	Sixth road section
1	65.59°	51.90°	106.48°	137.07°	147.56°	153.65°
2	65.77°	51.59°				
3	65.97°	51.62°				
4	66.24°	51.64°				
5	66.46°	51.34°				
6	66.85°	50.08°				
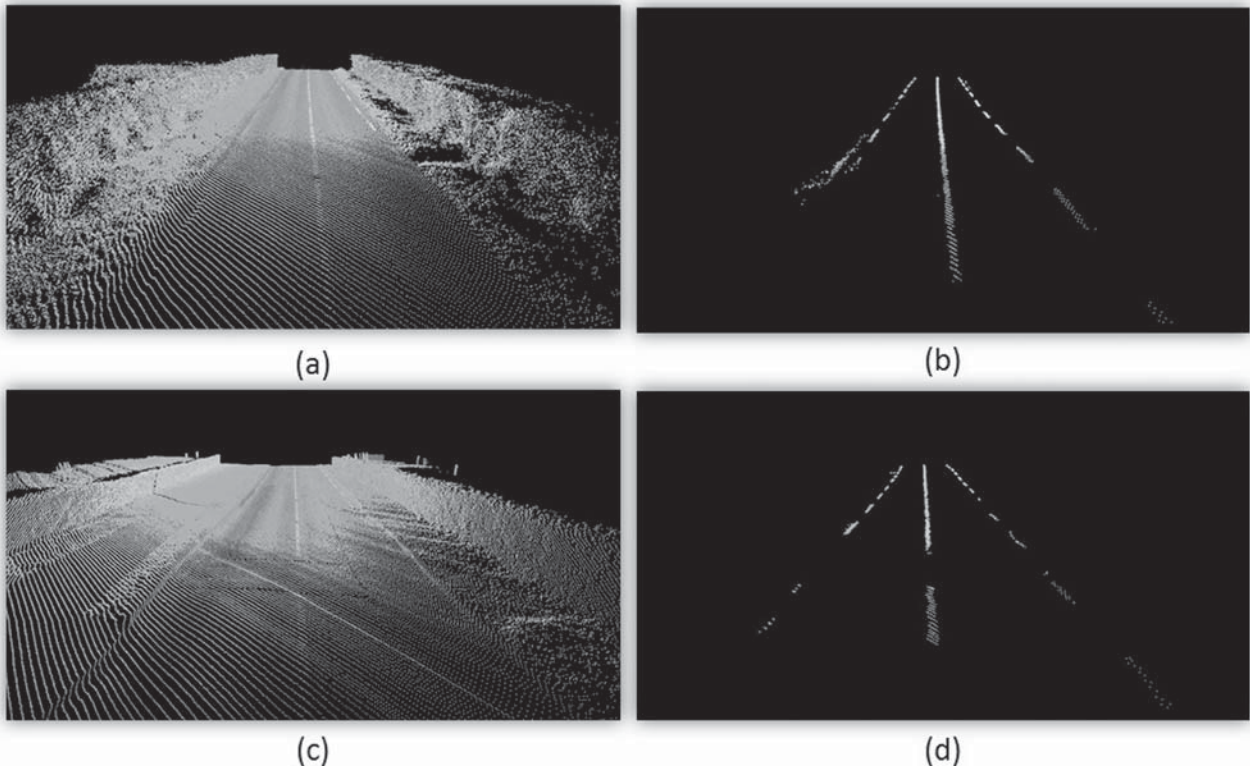
Fig. 11. 3D (a) LiDAR data and (b) extracted broken and continuous line markings of the 50 m first road section & 3D (a) LiDAR data and (b) extracted broken and continuous line markings of the 50 m second road section.
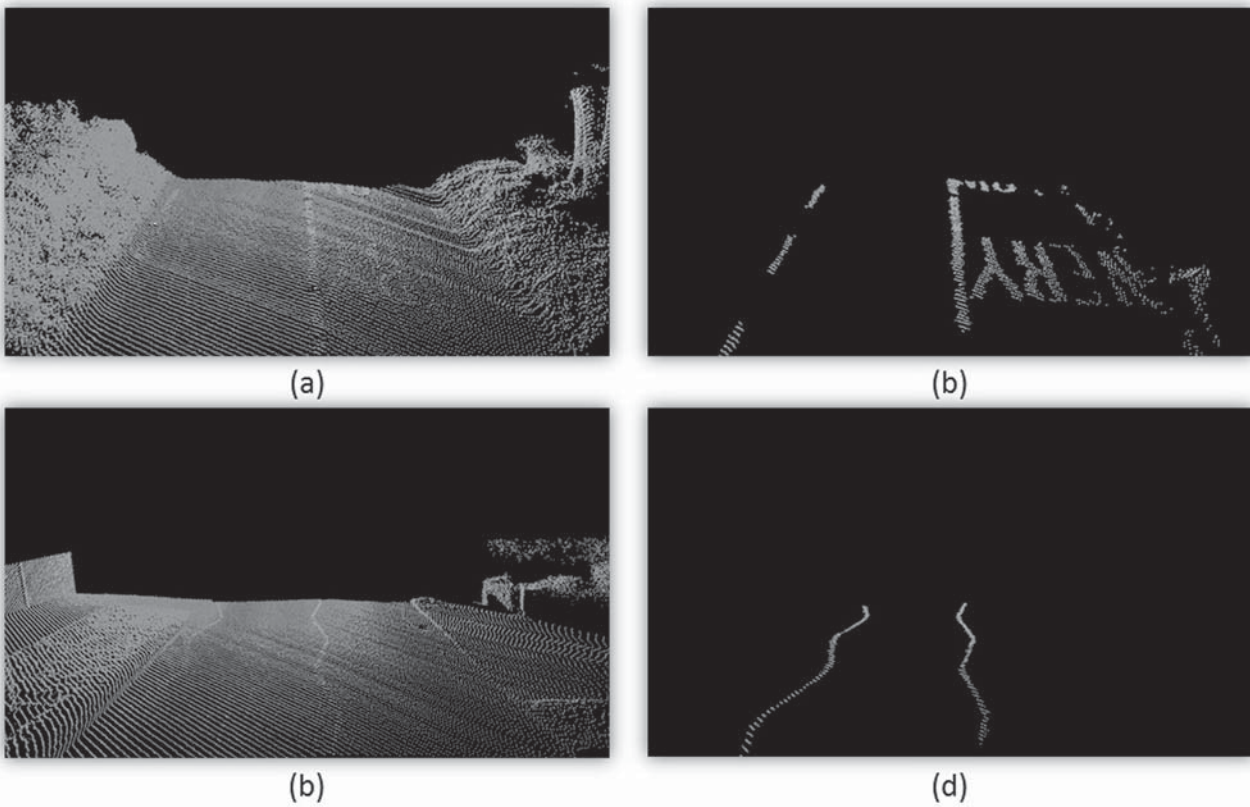
Fig. 12. 3D (a) LiDAR data and (b) extracted word, broken and continuous line markings of the 10 m third road section & 3D (a) LiDAR data and (b) extracted zig-zag markings of the 10 m fourth road section.
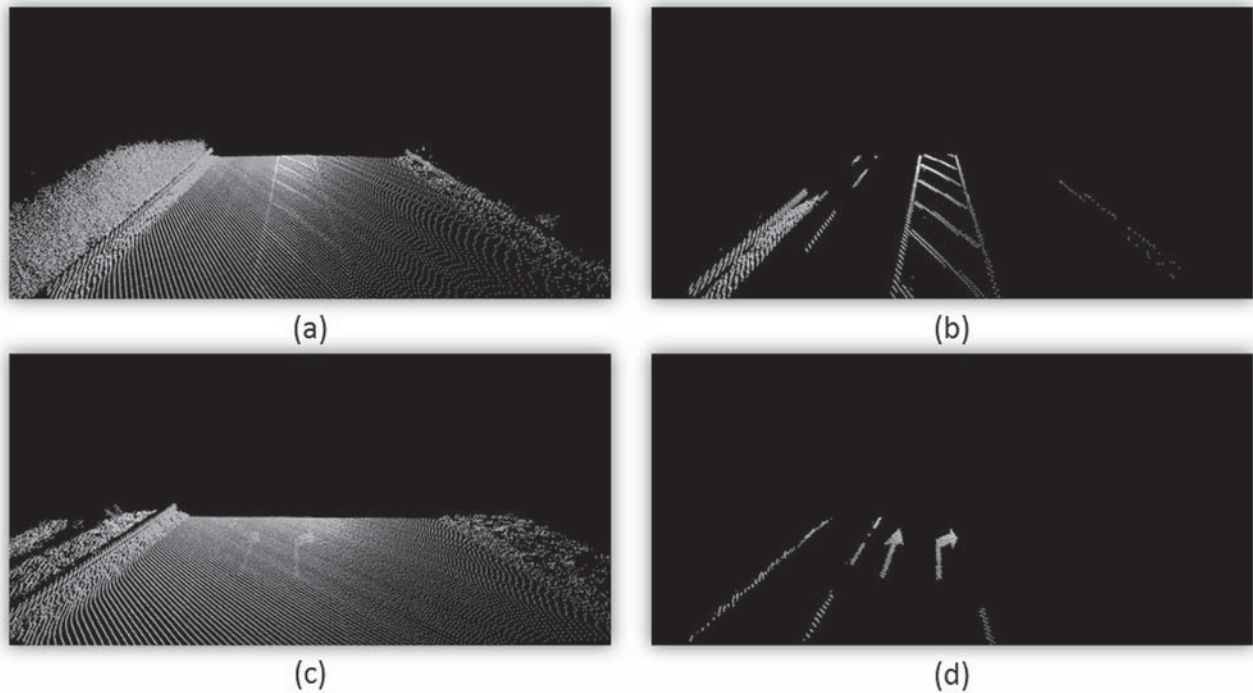
Fig. 13. 3D (a) LiDAR data and (b) extracted hatch and broken line markings of the 10 m fifth road section & 3D (a) LiDAR data and (b) extracted arrow and broken line markings of the 10 m sixth road section.
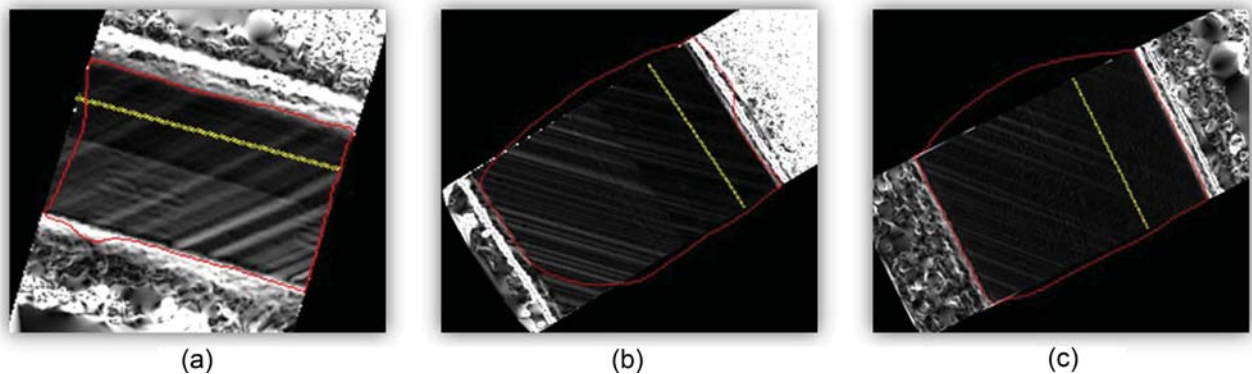
Fig. 14. The road boundaries extracted using automated road edge extraction algorithm in the (a) third, (b) fifth and (c) sixth road section are represented with red while the navigation points are represented with yellow. (For interpretation of the references to color in this figure legend, the reader is referred to the web version of the article.)

were missed. Thus, we were able to detect 90.91% of the road marking objects and 88.43% of the road marking points. We identified 10 groups of LiDAR points which were incorrectly labelled as extracted road markings on the basis of their length and width.

In the first and second road sections, our algorithm was able to extract the broken and continuous line markings. Some broken line markings along the left side of both road sections were not detected due to lower intensity values of the laser return from them. The extracted markings in the first road section contained some surface elements along the left edge, as seen in Fig. 11(a). This was primarily due to the road boundaries extracted using our automated road edge extraction algorithm which were extended incorrectly into a grass and soil area. The road boundaries extracted in the first 50 m rural and the second 50 m urban road section can be referred in Kumar et al. (2013). The LiDAR points belonging to grass and soil surface in the first road section produced high intensity values which were not removed by our road marking extraction algorithm due to their large physical dimension. The broken markings that were not detected along the right side of the second road section

were attributed to a lower point density of the LiDAR data along the right side. This was due to the use of a single laser scanner in the XP-1 system during the data acquisition process which led to the acquisition of LiDAR data with a lower point density along the right side of the road section than along its left side (Cahalane et al., 2011, 2012). The use of more than one laser scanner or a double pass approach in which the vehicle is driven back and forth on the road can be employed to acquire uniform and dense point cloud along both sides of the road section (Kumar et al., 2013). Our automated road marking extraction algorithm will provide an improved extraction of road markings using such LiDAR data.

In the third road section, the algorithm successfully extracted the majority of the word, broken and continuous line markings. The extracted road markings contained some surface elements along the right edge. This was due to the use of road boundaries, extending incorrectly into grass and soil area at some points, as shown in Fig. 14(a). Some of the extracted words along the right side were incomplete which was due to a lower LiDAR point density along that side of the road section. In the fourth road

section, our algorithm was able to extract two zig-zag markings but failed to detect the third one along the right side of the road section. This was again due to the lower point density of the LiDAR data along the right side of the road section.

Our algorithm was able to extract the hatch and broken line markings in the fifth road section. Surface elements present along the left side of the road section was due to the extracted road boundaries extending incorrectly into a grass and soil area, as can be seen in Fig. 14(b). In the sixth road section, the road marking extraction algorithm was able to extract the arrow and broken line markings. The broken line markings along the right side of the road section were not extracted due to a lower point density of the LiDAR data along that side. Surface elements in the form of a continuous line along the left side of the road section was due to the extracted road boundaries extending into the grass and soil area, as can be seen in Fig. 14(c). In the next section, we conclude the research work presented in this paper.

7. Conclusion

We presented an automated algorithm for extracting road markings from MLS data. The presented algorithm is based on the assumption that the LiDAR intensity return values from the road markings are higher than those from other road surface elements. The successful extraction of distinct road markings from the multiple tested road sections validates our automated algorithm. These research findings could contribute to a more rapid, cost-effective and comprehensive approach to the maintenance of road networks and ensure maximum safety conditions for road users.

We developed a range dependent thresholding function to extract the road markings from the intensity attribute. We select a single optimal threshold value and use it to automatically estimate the multiple range dependent threshold values. The use of proper normalised values of intensity attribute with respect to the range and incidence angle of the laser beam will allow us to select a single and robust threshold value for extracting road markings. This will remove the requirement of multiple range dependent threshold values in our algorithm. We made novel use of priori knowledge of the dimensions of road markings and binary morphological operations in order to complete their shapes and to remove other road surface elements introduced through the use of thresholding. The morphological operations are applied using the linear shaped structuring elements. Further research is required to investigate alternative structuring elements which could be useful in removing surface elements introduced through the use of extracted road boundaries, extending incorrectly into the grass and soil area. The output of our road marking extraction algorithm is a set of LiDAR points representing road marking objects. The shape, dimension and position on the road of these objects can be examined to construct more effective algorithms that could recognise and classify each road marking type.

Acknowledgements

References

Barber, D., Mills, J., Smithvoysey, S., 2008. Geometric validation of a ground-based mobile laser scanning system. ISPRS J. Photogram. Rem. Sens. 63 (1), 128–141.

Butler, D.A., 2011. Using GIS to automate the extraction of road markings for route corridor analysis. National University of Ireland Maynooth, pp. 1–78 (M.Sc. Dissertation).

Cahalane, C., Mccarthy, T., McElhinney, C.P., 2012. MIMIC: mobile mapping point density calculator. In: Proceedings of 3rd International Conference on Computing for Geospatial Research and Applications, Washington, 1–3 July, pp. 15:1–15:9.

Cahalane, C., McElhinney, C.P., McCarthy, T., 2011. Calculating the effect of dual-axis scanner rotations and surface orientation on scan profiles. In: Proceedings of 7th International Symposium on Mobile Mapping Technology, Krakow, 13–16 June, pp. 1–6.

Chen, X., Stroila, M., Wang, R., Kohlmeyer, B., Alwar, N., Bach, J., 2009. Next generation map making: geo-referenced ground-level LiDAR point clouds for automatic retro-reflective road feature extraction. In: Proceedings of 17th International Conference on Advances in Geographic Information Systems, Seattle, 4–6 November, pp. 488–491.

Clode, S., Kootsookos, P., Rottensteiner, F., 2004. The automatic extraction of roads from LiDAR data. Int. Arch. Photogram. Rem. Sens. Spat. Inform. Sci. 35 (Part B3), 1–6.

ETSC, 1997. Road safety audit and safety impact assessment. http://www.etsc.eu/oldsite/roadaudit.pdf (accessed 15.12.11).

Gatti, G., Polidori, C., Galvez, I., Mallschutzke, K., Jorna, R., Leur, M., Dietze, M., Ebersbach, D., Lippold, C., Schlag, B., Weller, G., Wyczynski, A., Iman, F., Aydin, C., 2007. Safety handbook for secondary roads. http://ec.europa.eu/transport/roadsafety_library (accessed 05.01.12).

Haala, N., Kada, M., 2010. An update on automatic 3D building reconstruction. ISPRS J. Photogram. Rem. Sens. 65 (6), 570–580.

Hammoudi, K., Dornaika, F., Paparoditis, N., 2009. Extracting building footprints from 3D point clouds using terrestrial laser scanning at street level. Int. Arch. Photogram. Rem. Sens. Spat. Inform. Sci. 38 (3/W4), 65–70.

Haralick, R.M., Shapiro, L.G., 1992. Computer and Robot Vision. Addison-Wesley, Reading.

Hu, X., Tao, C.V., Hu, Y., 2004. Automatic road extraction from dense urban area by integrated processing of high resolution imagery and lidar data. Int. Arch. Photogram. Rem. Sens. Spat. Inform. Sci. 35 (B3), 320–324.

Jaakkola, A., Hyyppä, J., Hyyppä, H., Kukko, A., Sep. 2008. Retrieval algorithms for road surface modelling using laser based mobile mapping. Sensors 8 (9), 5238–5249.

Jutzi, B., Gross, H., 2009. Normalization of LiDAR intensity data based on range and surface incidence angle. Int. Arch. Photogram. Rem. Sens. Spat. Inform. Sci. 38 (3/W8), 213–218.

Kaasalainen, S., Krooks, A., Kukko, A., Kaartinen, H., 2009. Radiometric calibration of terrestrial laser scanners with external reference targets. Rem. Sens. 1, 144–158.

Kabolizade, M., Ebadi, H., Ahmadi, S., 2010. An improved snake model for automatic extraction of buildings from urban aerial images and LiDAR data. Comput. Environ. Urban Syst. 34 (August (5)), 435–441.

Kumar, P., 2012. Road features extraction using terrestrial mobile laser scanning system. National University of Ireland Maynooth, pp. 1–300 (Ph.D. Dissertation).

Kumar, P., McCarthy, T., McElhinney, C.P., 2010. Automated road extraction from terrestrial based mobile laser scanning system using the GVF snake model. In: Proceedings of European LiDAR Mapping Forum, Hague, 30 November–1 December, pp. 1–10.

Kumar, P., McElhinney, C.P., Lewis, P., McCarthy, T., 2013. An automated algorithm for extracting road edges from terrestrial mobile LiDAR data. ISPRS J. Photogram. Rem. Sens. 85, 44–55.

Kumar, P., McElhinney, C.P., McCarthy, T., 2011. Utilizing terrestrial mobile laser scanning data attributes for road edge extraction using the GVF snake model. In: Proceedings of 7th International Symposium on Mobile Mapping Technology, Krakow, 13–16 June, pp. 1–6.

Lam, J., Kusevic, K., Mrstik, P., Harrap, R., Greenspan, M., 2010. Urban scene extraction from mobile ground based LiDAR data. In: Proceedings of 5th International Symposium on 3D Data, Processing, Visualization & Transmission, Paris, 17–20 May, pp. 1–8.

Li, J., Chapman, M.A., 2008. Terrestrial mobile mapping towards real time geospatial data collection. In: Zlatanova, S., Li, J. (Eds.), Geospatial Information Technology for Emergency Responses. Taylor & Francis Group, London, pp. 103–119.

Lin, Y.C., Mills, J.P., 2010. Factors influencing pulse width of small footprint, full waveform airborne laser scanning data. Photogram. Eng. Rem. Sens. 76 (1), 49–59.

McCarthy, T., McElhinney, C.P., 2010. European road safety inspection (EuRSI) research project. In: Proceedings of European Transport Conference, Glasgow, 11–13 October (on CD-ROM).

McElhinney, C.P., Kumar, P., Cahalane, C., McCarthy, T., 2010. Initial results from European road safety inspection (EURSI) mobile mapping project. Int. Arch. Photogram. Rem. Sens. Spat. Inform. Sci. 38 (5), 440–445.

Mumtaz, S.A., Mooney, K., 2009. A semi-automatic approach to object extraction from a combination of image and laser data. Int. Arch. Photogram. Rem. Sens. Spat. Inform. Sci. 38 (Part 3/W4), 53–58.

Oh, D., 2010. Radiometric Correction of Mobile Laser Scanning Intensity Data. International Institute for Geo-information Science and Earth Observation Enschede, pp. 1–77 (M.Sc. Dissertation).

Pecharda, C., Mariotta, C., Eggen, R., Toivonen, S., Brown, S., Matena, S., 2009. Safety at the heart of road design, pp. 1–10. http://www.eranetroad.org (accessed 05.12.11).

Pfeifer, N., Hofle, B., Briese, C., Rutzinger, M., Haring, A., 2008. Analysis of the backscattered energy in terrestrial laser scanning data. Int. Arch. Photogram. Rem. Sens. Spat. Inform. Sci. 37 (B5), 1045–1052.

Pu, S., Rutzinger, M., Vosselman, G., Elberink, S.O., 2011. Recognizing basic structures from mobile laser scanning data for road inventory studies. ISPRS J. Photogram. Rem. Sens. 66, 28–39.

Rutzinger, M., Elberink, S.J.O., Pu, S., Vosselman, G., 2009. Automatic extraction of vertical walls from mobile and airborne laser scanning data. Int. Arch. Photogram. Rem. Sens. Spat. Inform. Sci. 38 (W8), 7–11.

Samadzadegan, F., Bigdeli, B., Hahn, M., 2009. Automatic road extraction from LIDAR data based on classifier fusion in urban area. Int. Arch. Photogram. Rem. Sens. Spat. Inform. Sci. 38 (Part 3/W8), 81–86.

Schwarz, K.P., El-sheimy, N., 2007. Terrestrial and aerial mobile mapping systems. In: Tao, C.V., Li, J. (Eds.), Advances in Mobile Mapping Technology. Taylor & Francis Group, London, pp. 3–19.

Smadja, L., Ninot, J., Gavrilovic, T., 2010. Road extraction and environment interpretation from LiDAR sensors. Int. Arch. Photogram. Rem. Sens. Spat. Inform. Sci. 38 (3A), 281–286.

Toth, C., Paska, E., Brzezinska, D., 2007. Using pavement markings to support the QA-QC of LiDAR data. Int. Arch. Photogram. Rem. Sens. Spat. Inform. Sci. 36 (3/W49B), 173–178.

Toth, C., Paska, E., Brzezinska, D., 2008. Using road pavement markings as ground control for LiDAR data. Int. Arch. Photogram. Rem. Sens. Spat. Inform. Sci. 37 (B1), 189–196.

Transport, D., 2010. Traffic signs manual. http://www.transport.ie/viewitem.asp?id=13896&lang=ENG&loc=2635 (accessed 10.04.12).

Vain, A., Kaasalainen, S., Pyysalo, U., Krooks, A., Litkey, P., 2009. Use of naturally available reference targets to calibrate airborne laser scanning intensity data. Sensors 9, 2780–2796.

Vosselman, G., 2009. Advanced point cloud processing. In: Proceedings of Photogrammetric Week, Stuttgart, 7–11 September, pp. 137–146.

Yang, B., Fang, L., Li, Q., Li, J., 2012. Automated extraction of road markings from mobile LiDAR point clouds. Photogram. Eng. Rem. Sens. 78 (4), 331–338.

Zhou, L., Vosselman, G., 2012. Mapping curbstones in airborne and mobile laser scanning data. Int. J. Appl. Earth Observ. Geoinform. 18, 293–304.